Analysis of Hot Crack and Welding Deformation during One-side Butt Welding Using Idealized Explicit FEM

Tsuyoshi MIWA*1 · Dr. Kei YAMAZAKI*1 · Kensaku NISHIHARA*2 · Dr. Masakazu SHIBAHARA*3

*1 Technical Center, Welding Business
*2 KOBELCO WELDING TechnoSolutions Co., LTD
*3 Osaka Prefecture University (currently Osaka Metropolitan University)

Abstract

This paper reports on the analyses by idealized explicit FEM of hot crack and welding deformation during one-side butt welding. In the hot crack analysis, the incremental value of the plastic strain generated in the brittle temperature range (BTR) and the temperature gradient vector have been evaluated as the occurrence index of hot cracks. By comparing these with the results of welding experimentation, the validity and effectiveness of the hot crack occurrence forecasting by this analysis method have been examined. In the deformation analysis, the actual structure size level has been examined for one-side submerged arc welding (FCB™ method) and one-side tandem welding (HT-MAG™ method). It has been shown that the application of these analysis methods has enabled deformation forecasting at high speed and with high accuracy even in large-scale analyses, which hitherto have been difficult.

Introduction

The numerical simulation method has recently been widely used for the mechanical analysis of practical structures. In particular, the finite element method (hereinafter referred to as "FEM") is being introduced in a wide range of fields in design and production. However, the scope of its application to the analysis of welding mechanism is often limited to the vicinity of weld joints, and there are few examples of its application to large-scale analysis. This is because welding is a non-linear transient phenomenon accompanying moving heat sources. Currently, static implicit FEM is generally used to accurately simulate 3D stress/deformation behaviors. In this method, however, memory usage and analysis time become problems as the scale of the analysis increases. In addition, to analyze hot cracking during welding, it is necessary to accurately analyze the displacement and strain behavior of each part at a high temperature using small increments of time and temperature. If the object of analysis extends to welded joints and welded structures, the analysis will inevitably require an enormous amount of time.

An idealized explicit FEM, capable of analyzing at high speed with saved memory, has been applied to large-scale mechanical analysis. This study shows that this method effectively analyzes hot cracking during welding and welding deformations of actual structures.

1. Analysis method based on idealized explicit FEM for hot cracking

1.1 Analysis of welding mechanics by idealized explicit FEM

The following describes the analysis method of idealized explicit FEM, an FEM method for thermal elasto-plastic analysis with an increased scale and speed. Most conventional analyses of welding mechanics assume that the influences of inertial force and damping force are minor and employ the static implicit FEM to solve problems.

$$[M]\{\ddot{u}\}_t + [C]\{\dot{u}\}_t + [K]\{u\}_t = [F]_t \quad \cdots\cdots\cdots\cdots\cdots\cdots \quad (1)$$

The conventional method assumes that the influence of the first term (inertia term) and the second term (damping term) in the motion equation (1) are quasi-static phenomena that are negligibly small and solves the overall stiffness equation $[K]\lfloor u \rfloor_t = [F]_t$ expressed in incremental type. On the other hand, the idealized explicit FEM uses the temperature increment obtained by heat transfer analysis as the external force, and the load due to this temperature increment is given to Eq. (1). Solving Equation (1) using optimized mass matrix [M] and damping matrix [C] to increase analysis speed gives the displacement for the next step. In the idealized explicit FEM, the displacement calculation is advanced by solving the calculation step of dynamic explicit FEM, or the step in Equation (1). As the calculation step is advanced, the displacement converges to a constant value, and this step is repeated until the obtained displacement satisfies the static equilibrium, i.e., $[K]\lfloor u \rfloor_t = [F]_t$. After the static equilibrium is reached, the displacement is calculated in the following temperature step. In this way, the displacement calculation in the load step is regarded as a pseudo-dynamic problem, and the analysis is divided into pseudo-time steps for advancement. It should be noted that the static implicit FEM requires solving the stiffness

equation for the entire system, which makes the computational complexity in each calculation step enormous in a large-scale analysis. On the other hand, this idealized explicit FEM does not require solving the overall stiffness equation because it divides the calculation step to proceed with the analysis, and the computational complexity at each calculation step is much smaller than that of the static implicit FEM. Therefore, even if the number of steps to be calculated increases, it is possible to speed up the calculation and save memory.[1] In addition, in the thermal elasto-plastic analysis, the idealized explicit FEM advances the time step using dynamic explicit FEM until its solution reaches a state equivalent to the solution obtained by static implicit FEM, enabling an accuracy of analysis almost the same as that of the conventional method,[2] at a greater scale of analysis compared with the conventional method.[3]

1.2 Overview of hot cracking analysis method

Fig. 1 outlines the occurrence mechanism of hot cracking. Generally, metallic material has a brittle temperature range (hereinafter referred to as "BTR"), where ductility becomes extremely low at a temperature between liquidus and solidus. Hot cracking is considered to occur during the solidification process of welded metal when a significant strain occurs in the BTR with poor ductility. A proposed idea includes defining the minimum strain at which cracking occurs as the limit strain and evaluating the occurrence of cracking in the BTR by the strain acting on the welded metal and the high-temperature ductility curve.[4]

This study relates to the idealized explicit FEM analysis. As shown in **Fig. 2**, the increment of the plastic strain that occurs in the BTR between the liquidus and solidus temperatures, which depend on the material composition in the cooling process and are specified before analysis, is defined as the BTR plastic strain increment. This increment is considered the occurrence index of hot cracking to examine the influence of various factors on cracking.

The solidification morphology near the final solidification zone of welded metal significantly affects the hot cracking resistance. It has been experimentally confirmed that when the meeting angle between crystals is small and butting solidification (head-on collision solidification) occurs, an impurity segregation line appears and promotes cracking.[5] It should be noted that, except for the initial stage of solidification, the solidification growth direction of welded metal is approximately the same as the direction of the

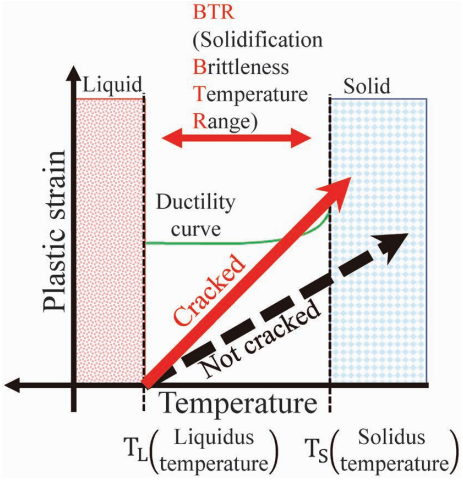

Fig. 1 Mechanism of hot cracking

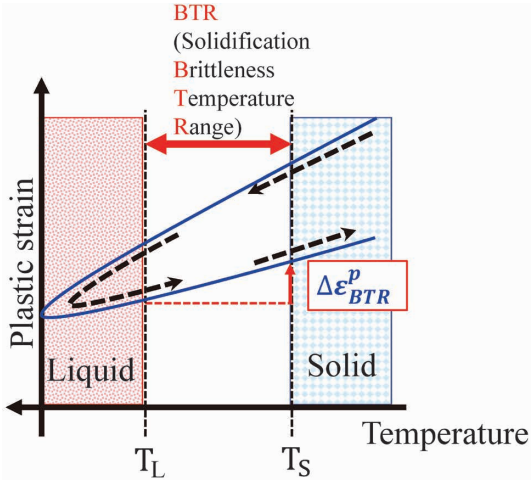

Fig. 2 Schematic illustration of plastic strain increment in BTR during cooling

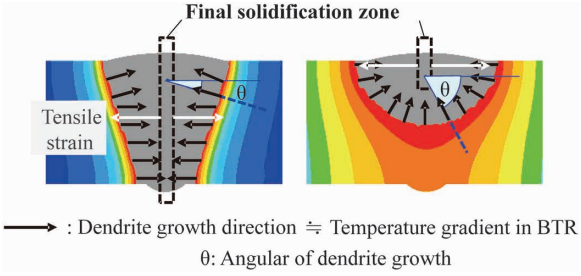

Fig. 3 Schematic illustration of BTR temperature gradient vector

maximum temperature gradient. Therefore, this study considers the solidification growth direction of welded metal and proposes a simple method to determine the direction of solidification growth from the temperature gradient vector obtained by heat transfer analysis. The temperature gradient vector when the liquidus temperature is passed through in the cooling process and transition is made into the BTR is defined as the BTR temperature gradient vector. The direction of this temperature gradient vector is assumed to be the solidification

growth direction. As shown in **Fig. 3**, evaluation is conducted on the angle formed between the temperature gradient vector at the position where the dendrites meet in the final solidification zone and the direction perpendicular to the welding line (hereinafter referred to as the dendrite growth angle).

2. Analysis of hot cracking in one-side tandem welding

One-side tandem welding is a method for realizing automation and high efficiency of welding in the plate joining process in shipbuilding. Regarding this welding, experiments have been conducted to accelerate hot cracking. Also carried out was an idealized explicit FEM to simulate the experiments. The following describes the results.

2.1 Testing method of cracking in one-side tandem MAG welding

Following JIS G 3106 SM490A, a small, simple trolley for automatic welding was used to perform single-side first-pass welding at the flat position on sample steel plates. The shape of the testing plates is shown in **Fig. 4**, the testing conditions are listed in **Table 1**, and the schematic diagram of the welding is depicted in **Fig. 5**. The points ①, ②, and ③ in Fig. 4 will be explained in Section 2.3. In-plane tack welding of 5 mm in height and 50 mm in length was provided to the welding ends and the central region of the welding line. For the stabilization and welding improvement of the molten pool, a cut wire for groove filling (FAMILIARC™ Note 1) M-GRITS, ϕ1.2 mm × 1.4 mm) was sprayed in the groove. FAMILIARC™ FB-B3 was attached to the entire back side of the welding line as a backing material. Flux-cored wires (hereinafter referred to as "FCW") were used for both electrodes. Arc interference was suppressed by using FAMILIARC™ MX-100E (polarity DCEP) for the leading electrode and FAMILIARC™ DW-1ST (polarity DCEN) for the trailing electrode. The electrode distance was 40 mm, the plate thickness was changed from 16 mm to 25 and 32 mm, and the hot cracking positions along the 600 mm length (excluding starting and runoff web tabs) of this weld were evaluated by X-ray transmission testing.

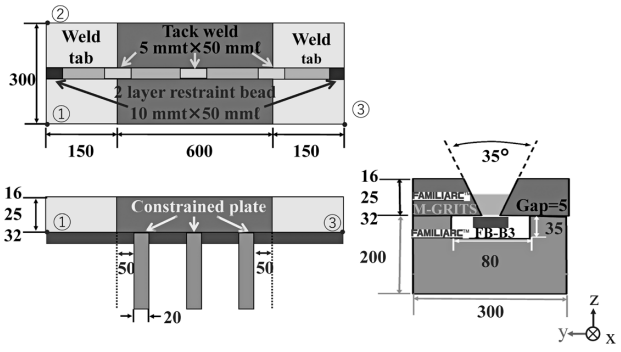

Fig. 4 Shape and dimensions of test plate

Table 1 Welding conditions

Electrode	Polarity	Wire	Welding current -arc voltage	Electrode distance	Welding speed
Leading	DCEP	FAMILIARC™ MX-100E (φ1.6)	410 A-34 V	40 mm	250 mm/min
Trailing	DCEN	FAMILIARC™ DW-1ST (φ1.4)	240 A-24 V		

2.2 Testing results of cracking in one-side tandem MAG welding

Fig. 6 shows the hot cracking test results. The 16 mm thick plate exhibits no hot cracking throughout the overall length of the welding line. The 25 mm thick plate, however, has hot cracking near the tack weld in the groove positioned in the center of the welding line, and the 32 mm thick plate has hot cracking also in places other than the tack weld. **Fig. 7** is a cross-sectional macrograph of the 25 mm thick plate at locations where cracking has occurred and where no cracking has occurred. Hot cracking has occurred in the upper region of the welded metal, and the dendrite growth angle at the cracking occurrence site is small. It should be noted that the distances from the welding metal surface are the same, even for the hot cracking that has occurred on

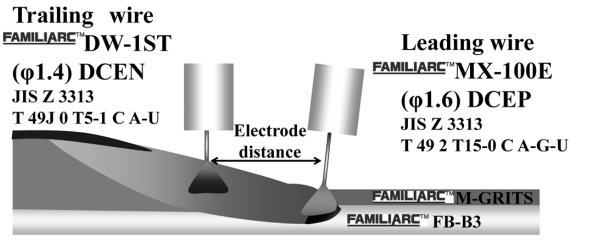

Fig. 5 Schematic illustration of one-side tandem MAG welding method

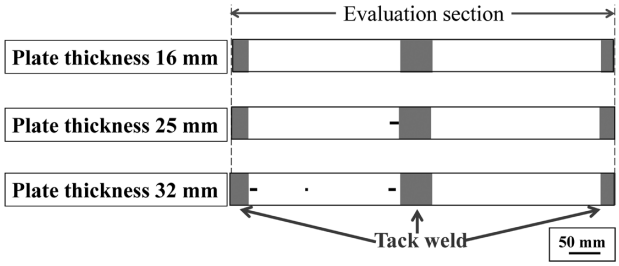

Fig. 6 Hot cracking test results

Note 1) FAMILIARC is a registered trademark of Kobe Steel.

the 32 mm thick plate. This result suggests that, in these welding conditions, the risk of hot cracking is particularly high near the tack weld and above the welded metal for the plate with a 25 mm or greater thickness.

2.3 Analysis of hot cracking in one-side tandem welding by idealized explicit FEM

An analysis model was created for the test plate shown in Fig. 4. The minimum mesh spacing in the cross-section near the weld was 0.5 mm, the mesh size in the welding line direction was 1 mm, and the number of nodes and element counts in the plate thickness of 25 mm were 1,122,416 and 1,059,664, respectively. The analysis time was 26 hrs. The material constants of SM490A shown in **Fig. 8** were used for the welded metal and base material. The analysis was performed at a BTR of 1,350 to 1,450 ℃. As the boundary condition, the back side was restrained at points ①, ②, and ③ in Fig. 4 in the xyz, xz, and z directions, respectively. This analysis does not take into consideration the influence of the latent heat of solidification.

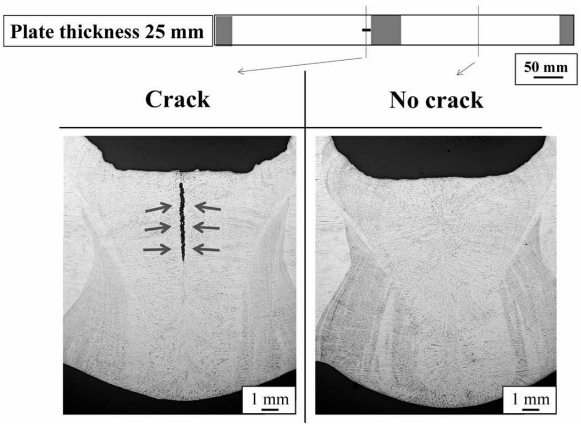

Fig. 7 Cross-sectional macrostructures

Fig. 9 shows the dendrite growth angle obtained by the analysis in the central region of the welded metal. Fig. 9 also includes the cross-sectional macrostructure corresponding to the analysis. At the plate thickness of 16 to 32 mm, the dendrite growth angle is negative in the region of 0 to 4 mm from the back bead surface, and the solidification growth direction is toward the lower region of the welded metal. On the other hand, in the region, 4 to 10 mm from the back bead surface, the dendrite growth angle becomes a positive value due to the heat input from the trailing electrode, and the direction of solidification growth is toward the upper region of

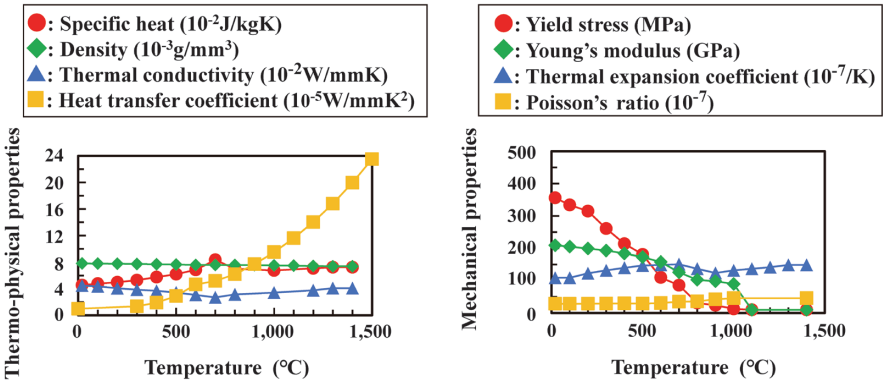

Fig. 8 Material constants

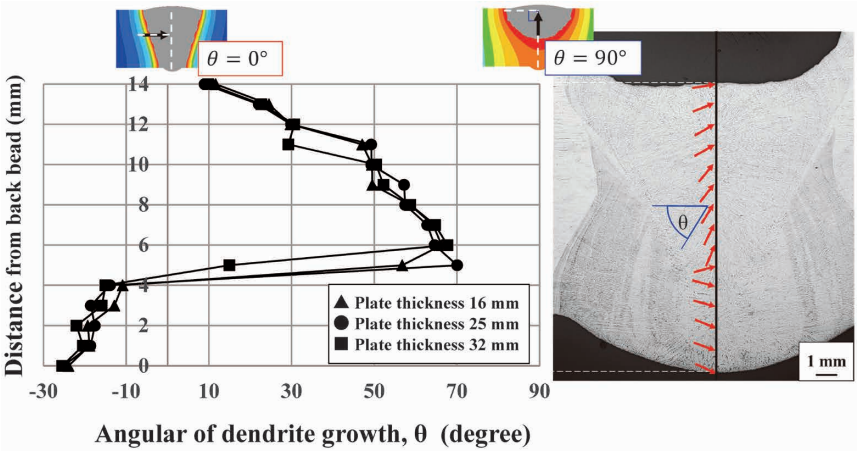

Fig. 9 Angular of dendrite growth

the welded metal. Meanwhile, in the experiment, the dendrite growth angle value is small in the vicinity of the welded metal surface where hot cracking occurred (the region 10 to 14 mm from the back bead), indicative of butting solidification (head-on collision solidification). Therefore, it is considered that the dendrite growth angle obtained by the above analysis roughly expresses the solidification morphology of the welded metal confirmed by the cross-sectional macrostructure shown in Fig. 9.

Fig.10 shows the distribution of BTR plastic strain increments in the cross-section of the welding line for each plate thickness. For the plate thickness of 16 mm, the BTR plastic strain increment does not become extremely large over the entire welding line, whereas, for the plate thicknesses of 25 mm and 32 mm, the BTR plastic strain increment becomes large near the tack weld positioned in the center of the welding line and the region above the welded metal.

Fig.11 shows the distribution of the BTR plastic strain increment and the distribution of the BTR temperature gradient vector in the cross-section of the tack weld (plate thickness 25 mm).

The BTR plastic strain increment in the upper region of the welded metal is shown to be relatively large. Also, the dendrite growth angle is smaller

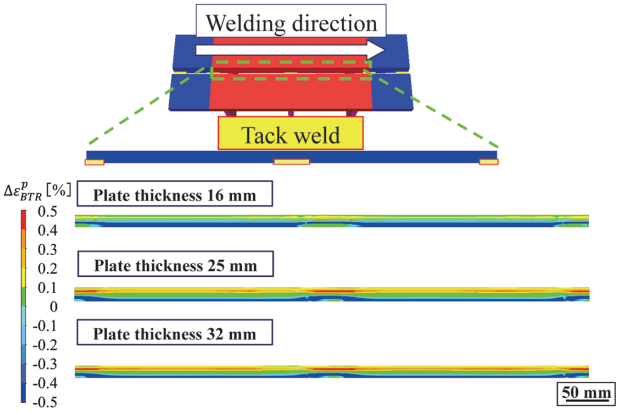

Fig.10 Distribution of BTR plastic strain increment in longitudinal section

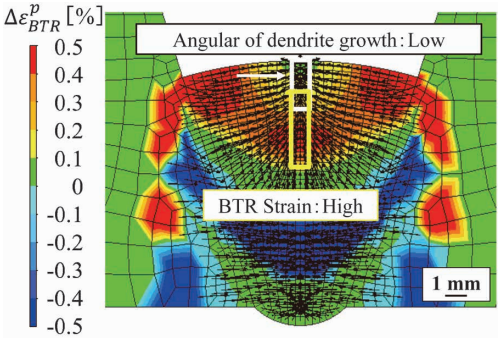

Fig.11 Distribution of the BTR plastic strain increment and the distribution of the BTR temperature gradient vector in the cross-section of the tack weld

in the upper region of the welded metal. In other words, the vicinity of the tack weld of a plate with a thickness of 25 mm or greater, where hot cracking occurred, is where the region with a significant BTR plastic strain increment and the region with a small dendrite growth angle overlap in the upper region of the welded metal. The result suggests that this analysis method can estimate the position with a high risk of hot cracking.

2.4 Considerations

A confirmation has been made on the angular distortion behavior obtained by this analysis and the cracking process in the cracked region. **Fig.12** shows the temperature change of the evaluation point near the tack weld caused by the heat-source movement and the transition of the angular distortion in the cross-section perpendicular to the welding line, including the evaluation point. Fig.12 (b) shows the calculation results of the angular distortion

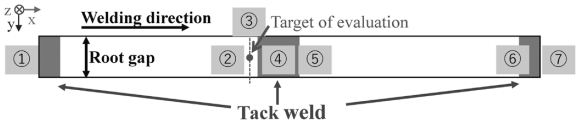

(a) Target point for evaluation and heat source locations

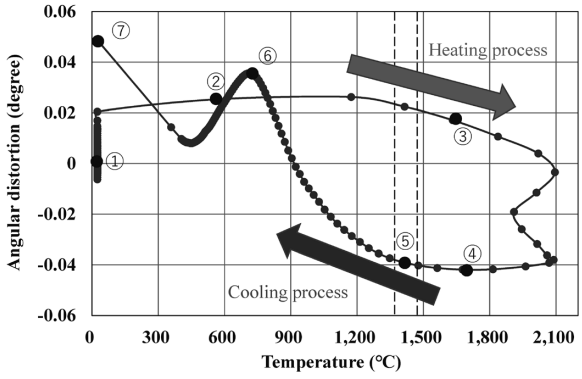

(b) Angular distortion and temperature behavior of near tack weld

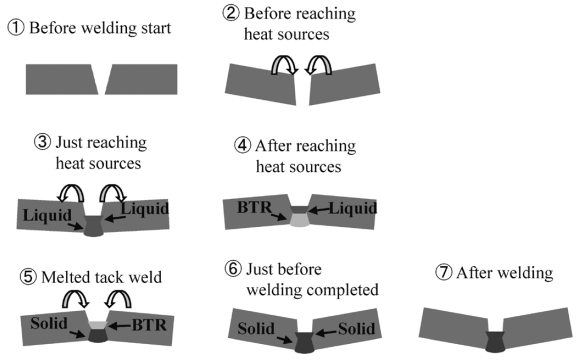

(c) Schematic illustrations of angular distortion behavior at each heat source location

Fig.12 Angular distortion behavior near tack weld portion

behavior when the heat source is positioned at ① to ⑦ in Fig.12 (a), and Fig.12 (c) depicts the schematic diagram. The temperature evaluation point is 2.3 mm from the upper surface of the welded metal where cracking occurred and 10 mm proximal to the tack welding end. The plate thickness is 20 mm, the center of the welding line is the adiabatic boundary surface, and a 1/2 symmetric model with a fixed y direction is used. Here, ① is before the start of welding, and angular distortion has not occurred. In ②, the heat source is located proximal to the evaluation point, and the cross-section of the evaluation point receives the influence of angular distortion of the existing weld. Here, the angular distortion has increased from a positive value because both ends of the base material rise, narrowing the groove angle, as shown in schematic diagram ②. Diagram ③ indicates the state when the heat source reaches directly above the evaluation point. The distortion angle is slightly reduced, and the groove angle is confirmed to have widened. This is attributable to the welded metal being in the liquid phase, and the vicinity of the heat source is thermally expanded. Diagram ④ shows the state after the heat source has passed the cross-section to be evaluated. The process from ③ to ④ causes a large deformation, changing the distortion angle from positive to negative. The welded metal begins solidifying from the lower region of the welded metal formed by the leading electrode. Since the upper region of the welded metal is in the liquid phase, the degree of restraint in the surrounding region is small, and the contribution to deformation is negligible. When the trailing heat source moves forward, and the upper region gradually solidifies, the thermal contraction in the upper region is restrained by the lower region that has already been solidified, leading to angular distortion. This is what causes such a large deformation to occur. Diagram ⑤ depicts the state after the heat source has passed through the tack weld and shows that the evaluation point is in the BTR. Here, the distortion angle tends to increase, and the groove angle narrows, as shown in diagram ⑤. At this time, the evaluation point is subjected to strain in the tensile direction. Then, when the tack weld has completely melted, the restraint due to the tack welding, which has suppressed the deformation of the plate until then and has been released, the strain rapidly increases in the direction of tearing the welded metal. As a result, as shown in Fig.11, the BTR plastic strain increment in the upper region of the welded metal near the tack weld becomes more significant than that in the steady region. Also, a large plate thickness is considered to increase the bending stiffness of the base material. As a result, the BTR plastic strain increment in the upper region of the welded metal over the entire welding line is considered to become more significant in the plate thickness of 25 mm and 32 mm than in the plate thickness of 16 mm, causing hot cracking. The diagram ⑥ shows the state before the end of welding. The distortion angle increases from ⑤ to ⑥, turning from a negative value to a positive value. Therefore, as shown in diagram ⑥, the groove angle narrows, resulting in a V-type angular distortion. The diagram ⑦ shows the state of cooling to room temperature after welding is completed. Immediately after ⑥, the tack welding of the welding terminal melts, and at that moment, the restraint that suppressed the expansion deformation near the heat source is released. Therefore, in the cross-section to be evaluated, the groove angle expands once from the V-type angular distortion. After the welding is completed, the welded metal contracts, resulting in a behavior in which the groove angle narrows, leading to a final deformed state, as shown in ⑦.

Thus, the influential factors in hot cracking are diverse, complex actions having to do with material type, welding heat input conditions, electrode distance, the groove condition, tack welding condition, restraint condition of the material, and the like. For this reason, even if the appropriate conditions for preventing hot cracking are extracted in the laboratory, hot cracking may occur in actual welding, and many trials and errors are often repeated on-site. This analysis method offers a valuable tool that proactively forecasts the positions with hot cracking risks in actual structures on the basis of simulation techniques introduced in the former section and offers welding guidelines on controlling various influential factors to suppress cracking.

3. Examples of welding deformation analysis aiming at actual structures

The FCB™ Note 2) method, which is one-side submerged arc welding, is widely applied in the plate joining process in shipbuilding. FCB™ is a method of single-sided welding, which includes spreading backing flux (FAMILIARC™ PF-I50R in this study) uniformly on a copper plate, pressing the copper plate against the back side of the groove with an air hose or by some other means, and performing multi-electrode submerged arc-welding using topside flux (FAMILIARC™ PF-I55E in this study) and wire (FAMILIARC™ US-36 in this study).

Note 2) FCB is a registered trademark of Kobe Steel.

On the other hand, the HT-MAG™ Note 3) method, which is two-electrode gas-shielded arc welding, has been developed in recent years to reduce welding deformation in the plate-joining process for thin steel plates (plate thickness of approximately 10 mm).[6] HT-MAG™ is a welding method using a solid wire, FAMILIARC™ MG-50HM, as the leading electrode for deep penetration, and FAMILIARC™ MX-50HM, which is an FCW for improving bead shape, as the trailing electrode. This paper introduces an example of analysis using idealized explicit FEM regarding the deformation reduction effect of HT-MAG™ on FCB™, targeting actual structures.

Fig.13 illustrates the target work for deformation analysis. The analysis has been conducted on the process of constructing a 15.8 m wide block using plates with a thickness of 9.5 mm. The weld length is 12 m, and three welding lines join the plates. The second and third welding passes are set to begin immediately after the end of the previous welding pass. The material constants of welded metal and base material are the same as in Fig. 8. The back sides of the points shown in ①, ②, and ③ in Fig.13 are restrained in the xyz, xy, and z directions, respectively, as the boundary conditions. **Fig.14** shows the cross-sectional shape of welded metal and the cross-sectional macrostructure after welding at the plate thickness of 9 mm in the analysis. The analysis has confirmed that the region heated to above 1,500 ℃ has a morphology similar to that of the cross-sectional macrostructure of the welded metal. **Table 2** shows the analysis conditions. The minimum mesh spacing in the cross-section near the weld is 1.5 mm, and the mesh size in the welding line direction is 10 mm. The number of nodes and element count for the FCB™ are 1,300,605 and 905,554, respectively, and the number of nodes and element count for the HT-MAG™ are 1,257,477 and 963,202, respectively. The welding heat input of HT-MAG™ is approximately 1/3 of that of FCB™, but these one-pass welding methods yield excellent penetration shape. **Fig.15** shows the displacement amount in the thickness direction after the end of the first welding pass, and **Fig.16** shows the amount of displacement in the thickness direction after the end of the third pass (final welding pass). It should be noted that the amount of displacement in the thickness direction is based

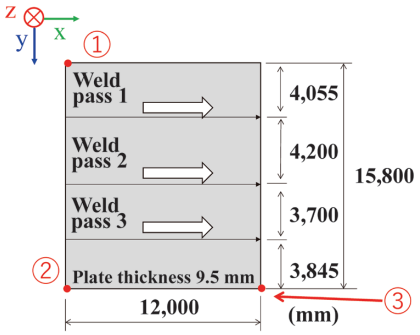

Fig.13 Shape and dimensions for deformation analysis

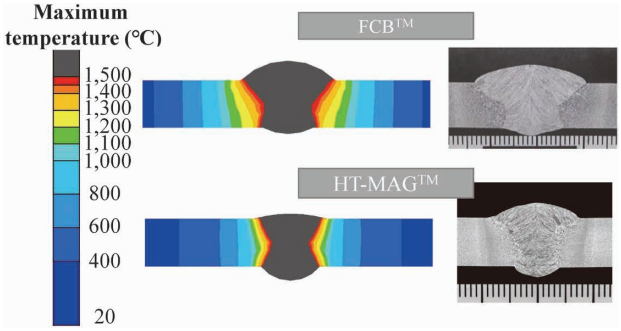

Fig.14 Cross-sectional shape in analysis

Table 2 Analysis conditions of FCB™ and HT-MAG™

	Leading electrode	Trailing electrode 1	Trailing electrode 2	Welding speed	Total heat input	Number of nodes	Number of elements
FCB™	1020 A-33 V	700 A-40 V	700 A-45 V	800 mm/min	6.99 kJ/mm	1,300,605	905,554
HT-MAG™	460 A-32 V	250 A-28 V	—	600 mm/min	2.14 kJ/mm	1,257,447	963,202

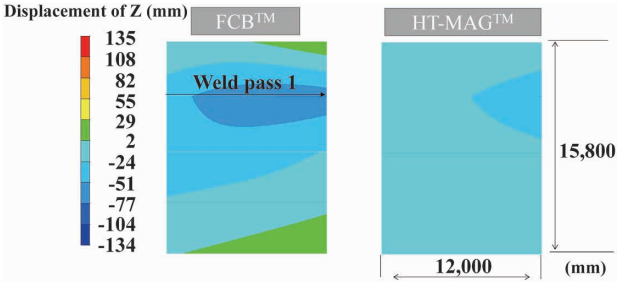

Fig.15 Displacement in thickness direction after first pass welding

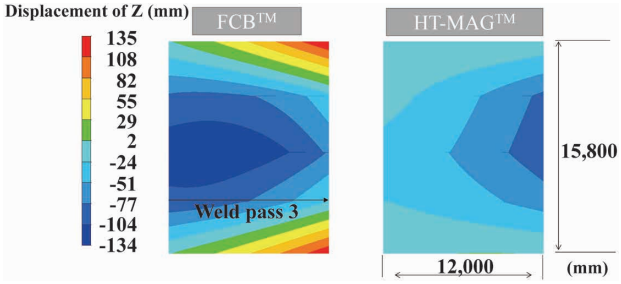

Fig.16 Displacement in thickness direction after third pass welding

Note 3) HT-MAG is a registered trademark of Kobe Steel.

on the back side of the plate before welding. In addition, for the convenience of calculation, the deformation of the third and fourth plates, which are unwelded, follows the deformation due to the first and second plates' first welding. The same applies to the second welding. HT-MAG™ has resulted in a minor displacement in the thickness direction over the entire plate. **Fig.17** shows the angular distortion at the center of the welding line (X = 6000). Both welding methods have resulted in V-type angular distortions, in which the difference between the maximum and minimum values in the thickness directions is 63 mm for HT-MAG™ and 185 mm for FCB™. The value for HT-MAG™ is approximately 1/3 of the value for FCB™. **Fig.18** shows the longitudinal bending deformation based on the welding start. Since the shape of welding metal differs depending on the welding method, a comparison has been made on the amount of longitudinal bending deformation in the center of the third plate, which is the center of the base material. These welding methods result in different deformation directions; HT-MAG™ causes deformation that descends as it progresses in the welding direction, whereas FCB™ causes a deformation that conversely ascends. Since the reference line cannot be fixed to compare the amount of longitudinal bending deformation, the amount of displacement from the tangent at X = 0 is used for the convenience of calculation. The maximum displacement from the tangent is 23 mm for HT-MAG™ and 82 mm for FCB™, confirming that the maximum displacement in longitudinal bending of HT-MAG™ is 1/3 that of FCB™ or less.

Although welding deformation is greatly influenced by the welding heat input, the deformation behavior is also affected by other factors such as the number of electrodes, electrode distance, groove conditions, restraint conditions, and welding sequence. The present analysis method has completed the deformation analysis in actual size (analysis example 2 above) in about 157 hrs. The time spent by the static implicit FEM with the same mesh is assumed to be more than 100 times longer. The idealized explicit FEM is regarded as a very effective method in the welding assembly analysis of large-scale structures, which hitherto has been considered difficult.

Conclusions

This paper has reported on hot cracking analysis using idealized explicit FEM and a method for analyzing the welding deformation of actual-sized structures. The results are shown below:

(1) In the hot cracking analysis, the incremental value of the plastic strain and the temperature gradient vector in the BTR have been evaluated as the hot cracking occurrence index. Comparison with the results of the

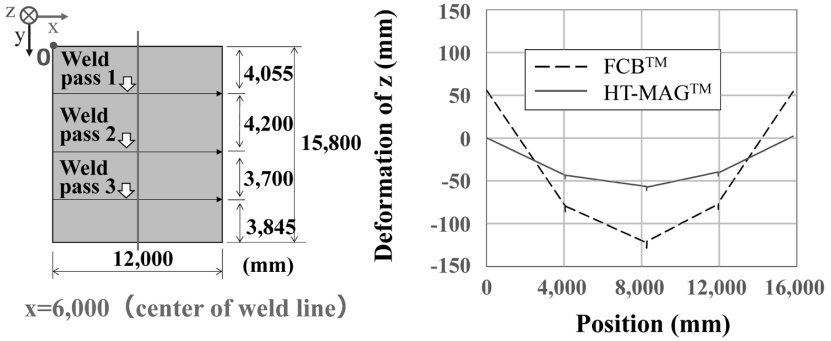

Fig.17 Analysis results of angular deformation

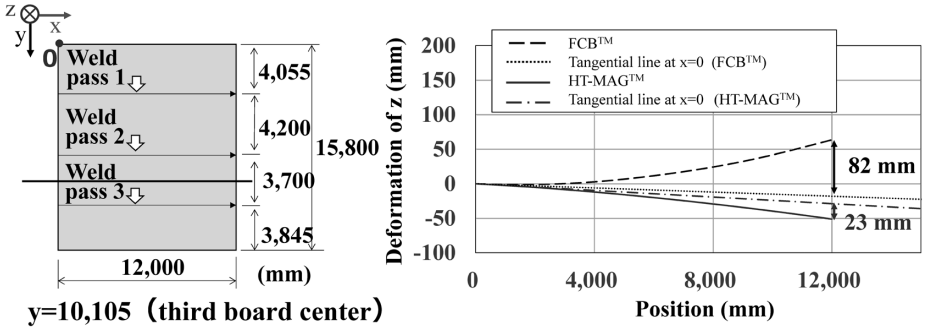

Fig.18 Analysis results of longitudinal bending deformation

welding experiment suggests that the occurrence of hot cracking can be forecasted by applying this analysis method.

(2) In the deformation analysis, FCB™ and HT-MAG™ have been used to conduct a study aiming at actual-sized structures. It has been shown that this analysis method enables high-speed, highly-accurate deformation forecasting even for large-scale analysis, which hitherto has been difficult.

Many welding problems are challenging to solve in the laboratory, "forecasting" and "performance evaluation" by the analysis method shown in this study are also considered to provide some welding solutions. Kobe Steel will strive to contribute to our customers' manufacturing by utilizing various welding solutions.

References

1) M. Shibahara et al. JOURNAL OF THE JAPAN WELDING SOCIETY. 2014, Vol.83, No.7, pp.549-554.
2) K. Ikushima et al. QUARTERLY JOURNAL OF THE JAPAN WELDING SOCIETY. 2013, Vol.31, No.1, pp.23-32.
3) K. Ikushima et al. QUARTERLY JOURNAL OF THE JAPAN WELDING SOCIETY. 2015, Vol.33, No.1, pp.69-81.
4) T. Senda et al. JOURNAL OF THE JAPAN WELDING SOCIETY. 1972, Vol.41, No.6, pp.709-723.
5) T. Kakizaki et al. Preprints of the National Meeting of JWS. 2017-9-11/13, JOURNAL OF THE JAPAN WELDING SOCIETY. 2017, pp.418-419.
6) Y. Yuan. R&D Kobe Steel Engineering Reports. 2018, Vol.67, No.1, pp.5-10.